– SUPPORTING INFORMATION –

Origin of the π-π Spacing Change upon Doping of Semiconducting Polymers

Wenlan Liu[1,2,3,§], Lars Müller[2,4,5,§], Shuangying Ma[2,3], Stephen Barlow[6], Seth R. Marder[6], Wolfgang Kowalsky[2,4], Andreas Köhn[2,3,], and Robert Lovrincic[2,4,*]*

[§] Both authors contributed equally to this work.

[1] Chongqing Key Laboratory of Green Synthesis and Applications & College of Chemistry, Chongqing Normal University, Chongqing 400047, China

[2]InnovationLab, Speyerer Str. 4, D-69115 Heidelberg, Germany

[3]Institute for Theoretical Chemistry, University of Stuttgart, Pfaffenwaldring 55, D-70569 Stuttgart, Germany

[4]Institute for High-Frequency Technology, TU Braunschweig, Schleinitzstr. 22, D-38106 Braunschweig, Germany

[5]Kirchhoff Institute for Physics, Heidelberg University, Im Neuenheimer Feld 227, D-69120 Heidelberg, Germany

[6]Center for Organic Photonics and Electronics and School of Chemistry and Biochemistry, Georgia Institute of Technology, Atlanta, GA 30332-0400, USA

1. Electron Diffraction Dosage Series of P3HT:F_4TCNQ

Figure S1 displays normalized radial profiles of electron diffraction patterns of pristine P3HT and P3HT:F_4TNCQ, recorded with different electron dosages (defined by the illumination time). For all measurements, the samples were cooled with liquid nitrogen. The position of the diffraction peak at 0.380 that represents the π-π spacing does not change for pristine P3HT for varying illumination times, shown for 200 ms and 2000 ms. However, for F_4TCNQ-doped P3HT, a clear signature of two peaks is visible for short illumination times, reproducing the results of studies performed with X-ray diffraction.[1–6] This signature can be observed with both sequential deposition of the dopant from acetonitrile (seq-s) and the mixed doping technique (mix), where P3HT and F_4TCNQ solutions are mixed prior to spin coating. For higher dosages, the double-peak structure gradually decreases, which could explain why previous studies with electron diffraction at room temperature did not or only slightly observe it.[7,8] In contrast to P3HT:F_4TNCQ, doping of P3HT with Mo(tfd-CO_2Me)$_3$ does not result in two distinct peaks (see Figure S2).

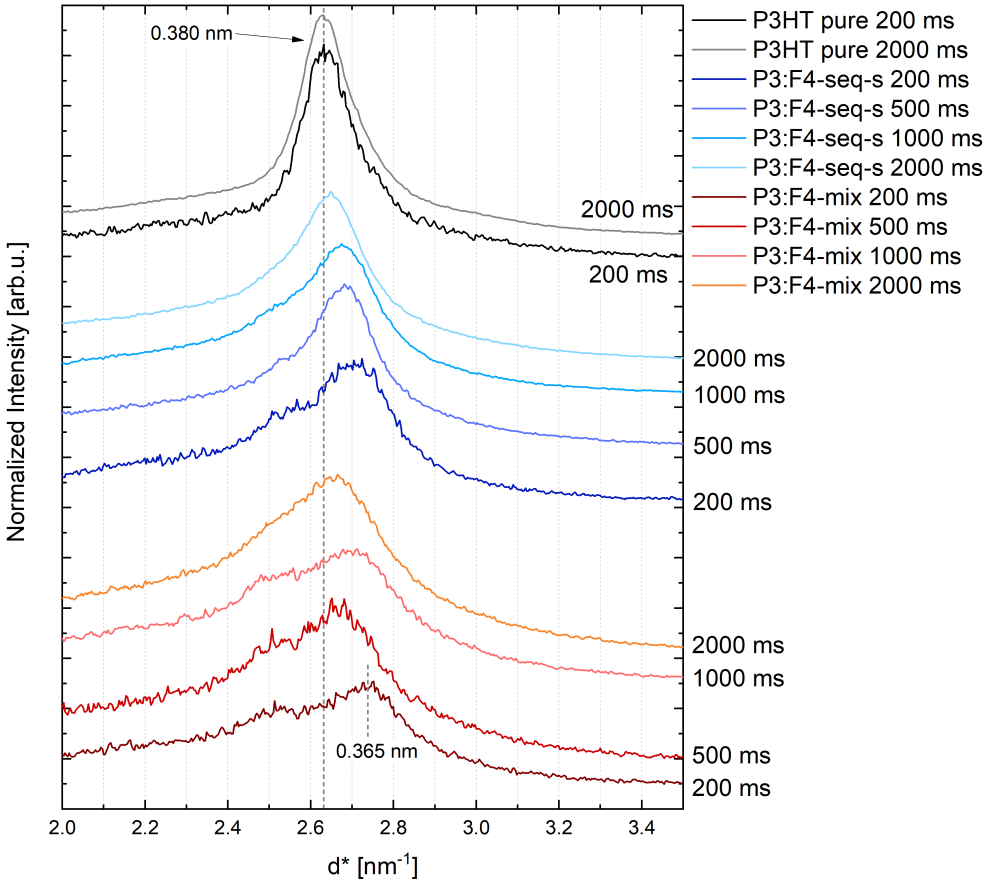

Figure S1. Normalized radial profiles of electron diffraction patterns of (liquid nitrogen-cooled) undoped P3HT and P3HT:F_4TCNQ thin films. The profiles were shifted in y-direction for clarity. The illumination time corresponding linearly to the electron dosage is given in milliseconds. P3: P3HT, F4: F_4TCNQ, seq-s: sequential doping from acetonitrile solution, mix: host and dopant solutions are mixed prior to spin coating.

2. Electron Diffraction Dosage Series of P3HT:Mo(tfd-CO_2Me)$_3$

Figure S2 displays normalized radial profiles of electron diffraction patterns of pristine P3HT and P3HT:Mo(tfd-CO_2Me)$_3$, recorded with different electron dosages (defined by the illumination time). For all measurements, the samples were cooled with liquid nitrogen. It can be seen that in contrast to P3HT:F_4TNCQ, doping with Mo(tfd-CO_2Me)$_3$ does not result in two distinct peaks. Instead, only one diffraction peak is observed, which is shifted to a larger d*, and hence a smaller π-π spacing. The position of this peak does not change with increasing electron dosage, comparable with the behavior of pristine P3HT. A similar peak position and dosage dependence is observed for mixed doping (mix), sequential doping from thermal evaporation of the dopant in vacuum onto a P3HT thin film (seq-v), and sequential doping from acetonitrile solution (seq-s).

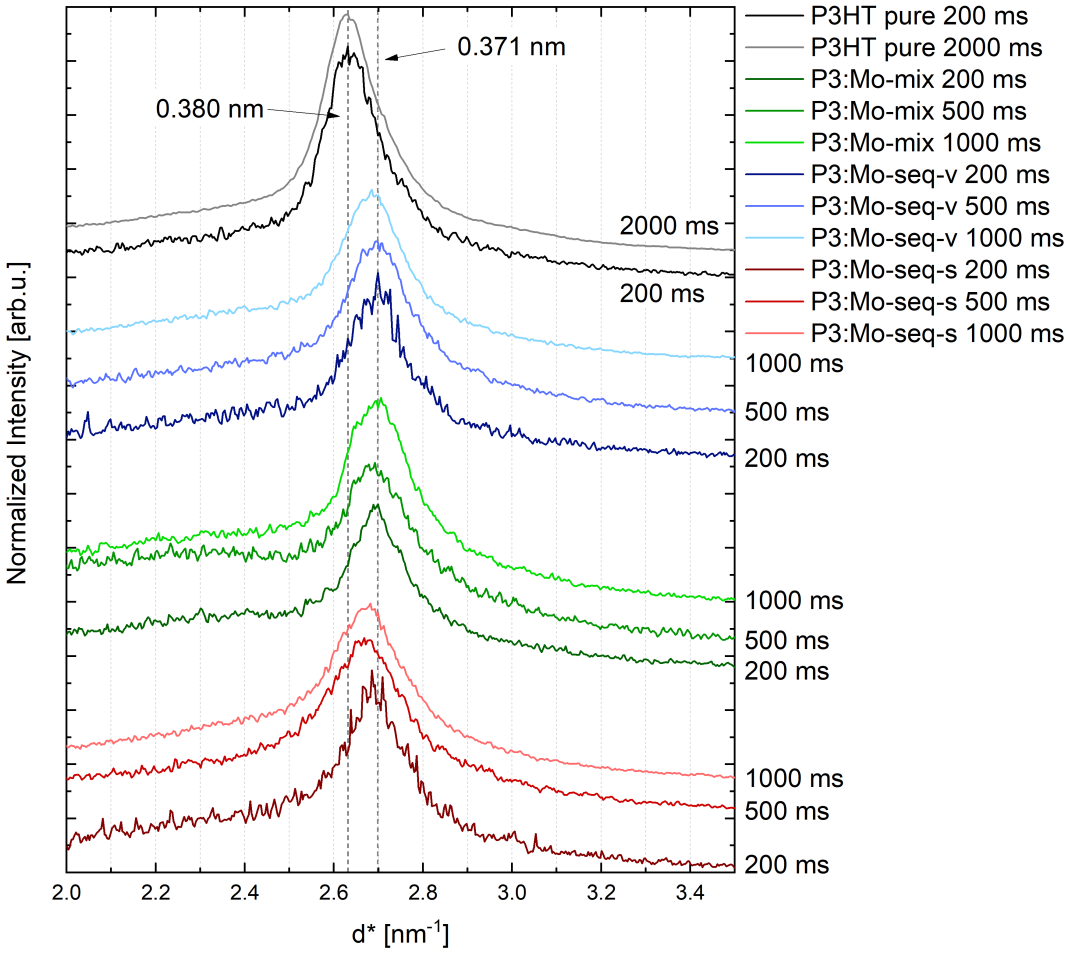

Figure S2. Normalized radial profiles of electron diffraction patterns of (liquid nitrogen-cooled) undoped P3HT and P3HT:Mo(tfd-CO_2Me)$_3$ thin films. The profiles were shifted in y-direction for clarity. The illumination time corresponding linearly to the electron dosage is given in milliseconds. P3: P3HT, Mo: Mo(tfd-CO_2Me)$_3$, seq-s: sequential doping from acetonitrile solution, seq-v: sequential doping via thermal evaporation of the dopant in vacuum conditions, mix: host and dopant solutions are mixed prior to spin coating.

3. Fit to low Dosage Electron Diffraction Profiles of P3HT:F_4TNCQ

Figure S3 shows radial profiles of electron diffraction patterns of pristine regioregular P3HT and regiorandom P3HT (P3HTrra), which develops an amorphous microstructure without crystallites. It can be seen that the broad background underneath the π-π spacing diffraction peak (010) around 2.5 nm^{-1} originates from the amorphous content of the film.[9] To estimate the intensity of the two peaks that are observed in case of P3HT:F_4TNCQ, a diffraction measurement of P3HTrra was used as baseline with a scalar factor regulating the intensity.

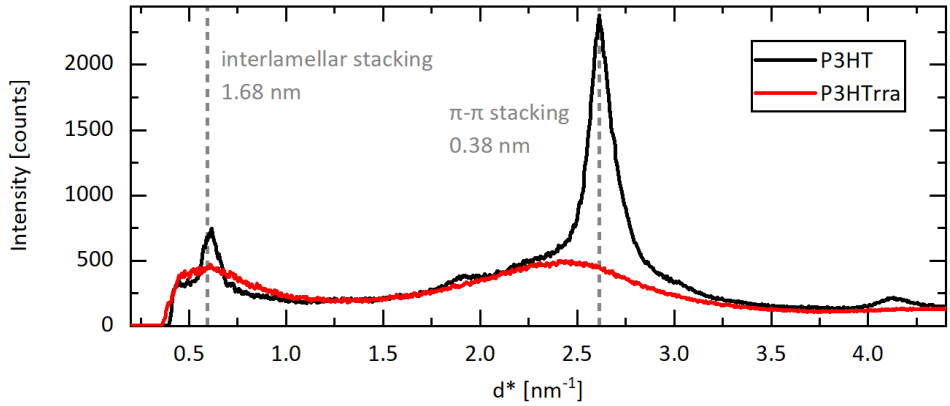

Figure S3. Radial profiles of electron diffraction patterns of thin films made of P3HT and regiorandom P3HT (P3HTrra). The samples were cooled with liquid nitrogen during measurements.

Figure S4 displays fits of the electron diffraction profiles of P3HT:F_4TNCQ-mix and –seq-s, recorded with 200 ms illumination time (compare Figure S1), in the region of the π-π spacing diffraction peak between 1.5 nm^{-1} and 3.5 nm^{-1}. As outlined above, a baseline corresponding to the amorphous content of the P3HT was used, as well as two Lorentzians that represent the two peaks of interest. Figure S4 reveals that the peak at higher d* values is significantly more pronounced compared to what could be expected by inspection of the profile at first sight. This is caused by the broad maximum of the baseline which is comparable in position to this peak. The fits were performed with the software fityk.[10] The fit parameters are given in table S1.

Table S1. Fit-parameters of fits to P3HT:F_4TNCQ-mix and –seq-s shown in Figure S4.

		Peak 1	Peak 2		P3HTrra
P3HT:F_4TNCQ-mix	height	133.97	38.173	amplitude	0.254
	center	2.735	2.522		
	hwhm	0.1019	0.0590		
P3HT:F_4TNCQ-seq-s	height	216.97	59.34	amplitude	0.218
	center	2.713	2.542		
	hwhm	0.0910	0.0829		

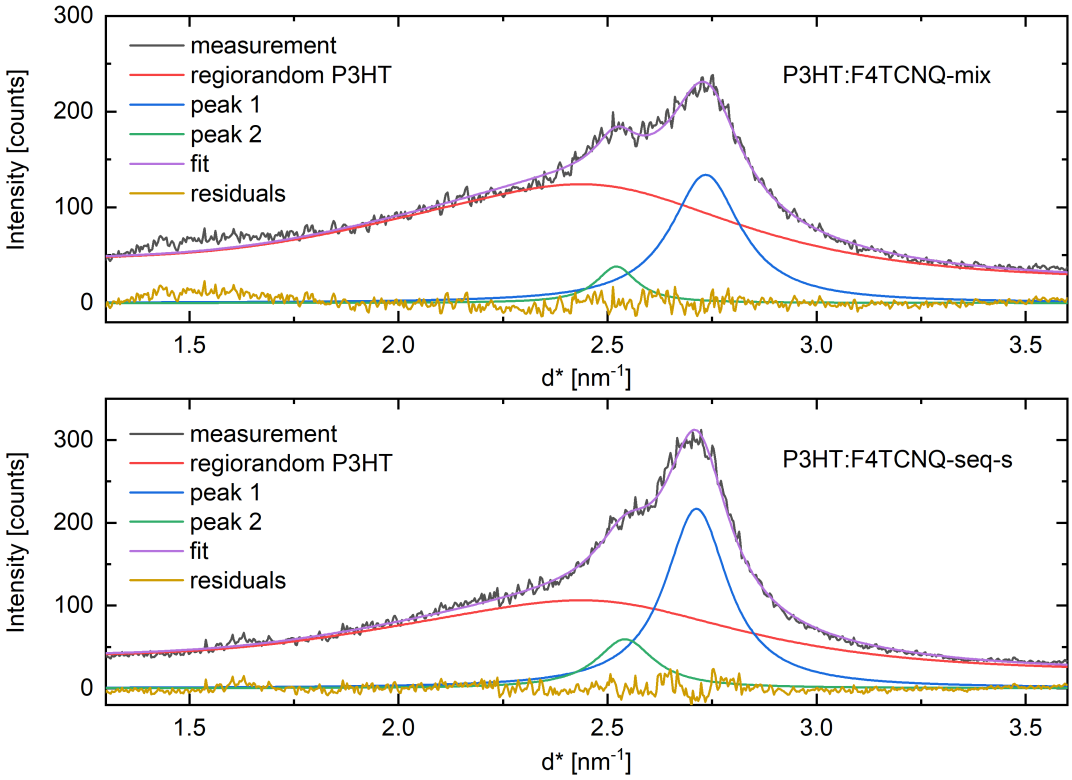

Figure S4. Fits to radial profiles of electron diffraction patterns of (liquid nitrogen-cooled) P3HT:F_4TNCQ thin films. *seq-s* describes sequential doping from acetonitrile solution, whereas *mix* refers to doping where host and dopant solutions are mixed prior to spin coating.

4. Bulk Structures of P3HT and Poly-thiophene

Fig. S5 shows the computed bulk structure of P3HT from side (upper) and top (lower) view. The bulk geometry is calculated with the VASP code[11,12] at the PBE[13] +D3 dispersion correction[14,15] level. (More computational details can be found in the article section: "DFT calculations".) The calculated parameters of the unit cell were: a=34.6 Å, b=7.2 Å, c=7.8 Å, α=89.4°, (angle between b and c axis), β=90.08°, γ=90.8°. The calculated stacking distance of the adjacent thiophene backbone planes is 3.45 Å.

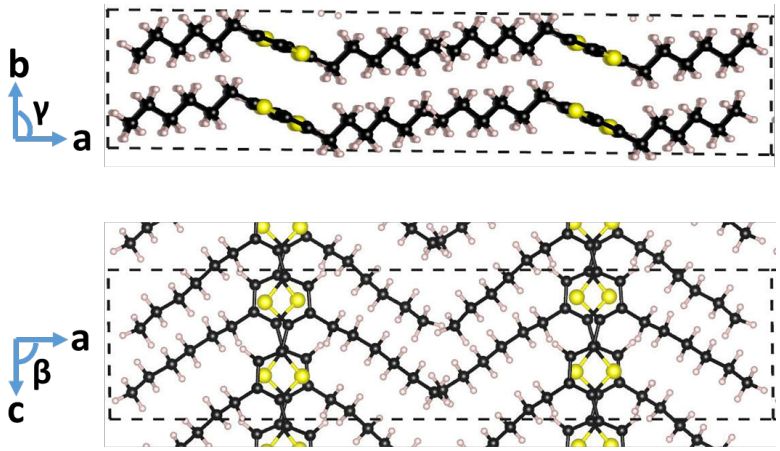

Figure S5. Computed bulk structure of P3HT. Top: View along b axis. Bottom: View along c axis.

The optimized bulk structure of poly-thiophene (Figure S6 left) has an approximately orthorhombic lattice with $P2_12_12_1$ pace group symmetry, in which all thiophene chains are stacked along the same axis of the unit cell. The planes of the thiophene chains in the same layer are parallel to each other, and the planes of the adjacent layers have an angle of θ=31°, leading to a classical herringbone structure.[16] The calculated cell parameters are: a=5.72 Å, b=7.76 Å, c=6.66 Å, α=90.2°, β=90.2°, γ=90.2°. The optimized poly-thiophene sheet (Figure S6 right) however maintains the π-π stacking structure (d=3.45Å) that is similar to the bulk P3HT, but with a slightly different registry of adjacent chains, as shown in the lower right part of Figure S6. A vacuum layer of thickness of 20 Å was added along the a direction. The structure was used to build a set of poly-thiophene dimers with shifted orientation of the rings, as used in the main text (Figure 4).

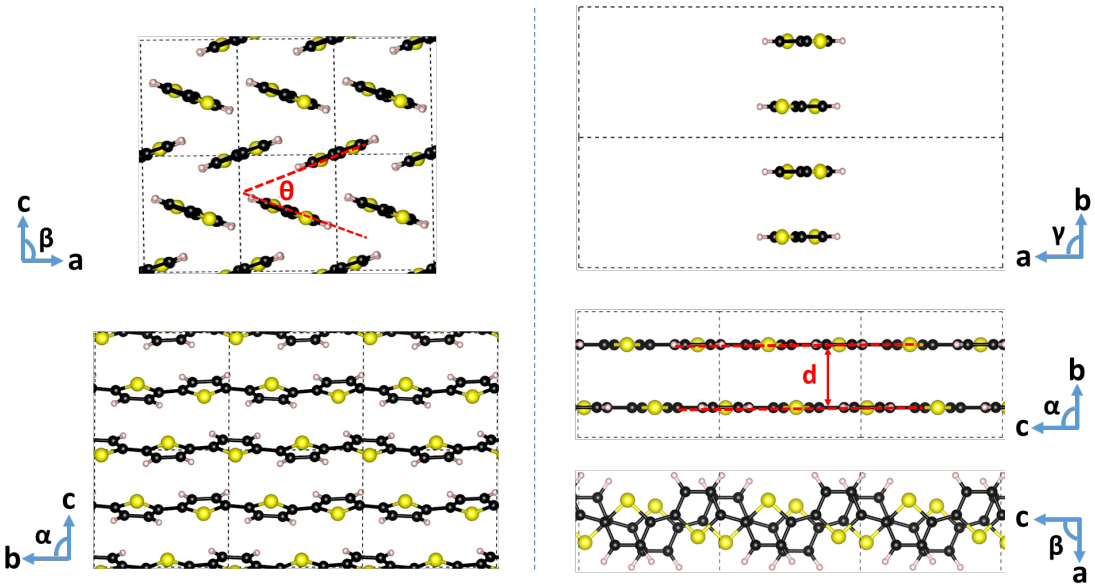

Figure S6. Left: computed structure of bulk poly-thiophene, from top to bottom are views along b and a axis, respectively; Right: computed structure of poly-thiophene nanoribbon, from top to bottom are views along b, a, c axis respectively.

5. Energy Decomposition Analysis

In order to distinguish between different effects such as electrostatic interaction or charge delocalization, we applied the energy decomposition analysis (EDA)[17,18] on a 4u π-π stacked poly-thiophene trimer system. The trimer is effectively considered as a dimer, where the closely stacked double chain and the third single chain are considered as the two subsystems. We designed two different initial cationic states, by assigning the positive charge to the single chain subsystem (cationic state I) or the double chain subsystem (cationic state II), respectively. By setting up an antisymmetrized and normalized product wavefunction of the system, we can calculate the electrostatic interaction energy (E_{elstat}) of a cationic single chain to a neutral single chain and the results are listed in Table S2. In our consideration, the exchange repulsion effect is included in the energy term E_{elstat}. The intermediate product wavefunction is further relaxed to the final state by allowing the monomer orbitals to mix with each other, and the corresponding interaction energy term is called orbital interaction energy (E_{orb}). The final states of the two EDA setups are energetically identical, where the cationic state I has a larger total interaction energy compared to the cationic state II. This means that the first EDA setup, where the positive charge is assign on a single chain, leads to an energetically higher lying initial state, therefore less favorable in terms of energy. All the interaction energy contribution terms, except the “orbital relaxation”, are very close to each other.

Table S2. Decomposition of the computed interaction energy (in kJ/mol) of the 4u poly-thiophene trimer at the equilibrium geometry of its cationic form. Cationic state I and II are the two different EDA initial state setups with the positive charge on the single chain subsystem (cationic state I) or the positive charge on the double chain subsystem (cationic state II).

	Cationic state I	Cationic state II
Total interaction energy	–160	–110
Electrostatic interaction + Pauli rep.	+178	+175
Orbital relaxation	–120	–75
Correlation interaction	–79	–74
Dispersion interaction	–138	–136

6. Charge Population of Large Model Systems Without Side Chains

Figure S7 shows how the two positive charges populate polythiophene tetramers, where all the tetramers adopted the equilibrium P3HT bulk structure and the side chains were substituted with H atoms. For small sized tetramers, i.e. 4u and 6u in length, the two positive charges delocalize on the whole chain of the upper and the lower poly-thiophene dimer, respectively. For medium sized tetramers, i.e. 8u and 10u, the two positive charges locate on the left and the right part of the upper and the lower poly-thiophene dimer chains, respectively. This also verifies that one positive charge is satisfied/populated in a 4u-5u thiophene dimer. For even larger dimers, the two positive charges delocalize on the left and the right part of poly-thiophene tetramer, respectively.

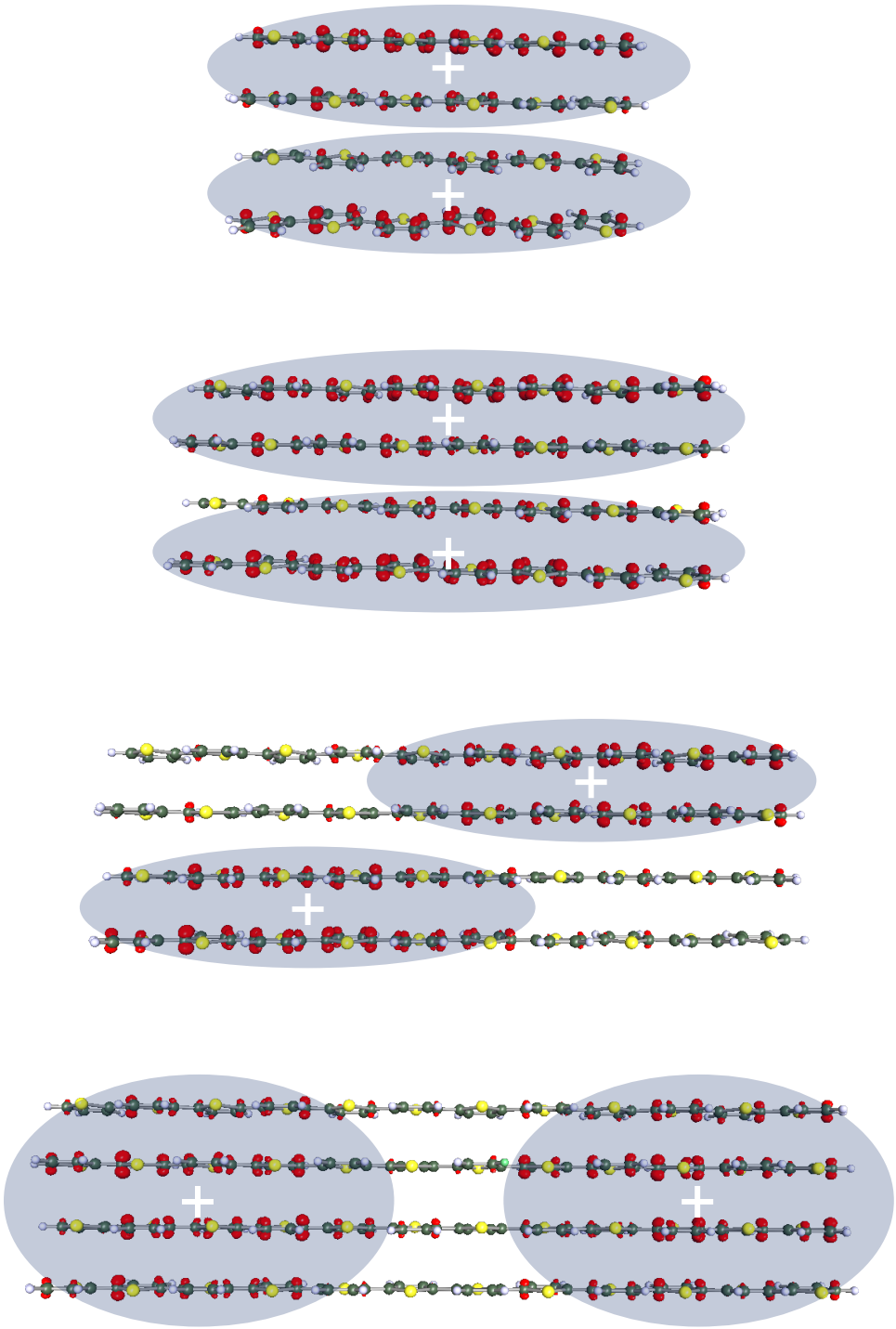

Figure S7. Charge population in poly-thiophene tetramers. From top to bottom: two positive charges delocalized on 6u, 8u, 10u, 12u tetramers, respectively.

References

(1) Scholes, D. T.; Yee, P. Y.; Lindemuth, J. R.; Kang, H.; Onorato, J.; Ghosh, R.; Luscombe, C. K.; Spano, F. C.; Tolbert, S. H.; Schwartz, B. J. The Effects of Crystallinity on Charge Transport and the Structure of Sequentially Processed F4TCNQ-Doped Conjugated Polymer Films. *Adv. Funct. Mater.* **2017**, *27*, 1702654.

(2) Lim, E.; Peterson, K. A.; Su, G. M.; Chabinyc, M. L. Thermoelectric Properties of Poly(3-Hexylthiophene) (P3HT) Doped with 2,3,5,6-Tetrafluoro-7,7,8,8-Tetracyanoquino-dimethane (F4TCNQ) by Vapor-Phase Infiltration. *Chem. Mater.* **2018**, *30*, 998-1010.

(3) Scholes, D. T.; Hawks, S. A.; Yee, P. Y.; Wu, H.; Lindemuth, J. R.; Tolbert, S. H.; Schwartz, B. J. Overcoming Film Quality Issues for Conjugated Polymers Doped with F4TCNQ by Solution Sequential Processing: Hall Effect, Structural, and Optical Measurements. *J. Phys. Chem. Lett.* **2015**, *6*, 4786-4793.

(4) Duong, D. T.; Wang, C.; Antono, E.; Toney, M. F.; Salleo, A. The Chemical and Structural Origin of Efficient P-Type Doping in P3HT. *Org. Electron.* **2013**, *14*, 1330-1336.

(5) Duong, D. T.; Phan, H.; Hanifi, D.; Jo, P. S.; Nguyen, T.-Q.; Salleo, A. Direct Observation of Doping Sites in Temperature-Controlled, p-Doped P3HT Thin Films by Conducting Atomic Force Microscopy. *Adv. Mater.* **2014**, *26*, 6069-6073.

(6) Thelen, J. L.; Wu, S.-L.; Javier, A. E.; Srinivasan, V.; Balsara, N. P.; Patel, S. N. Relationship between Mobility and Lattice Strain in Electrochemically Doped Poly(3-Hexylthiophene). *ACS Macro Lett.* **2015**, *4*, 1386-1391.

(7) Müller, L.; Nanova, D.; Glaser, T.; Beck, S.; Pucci, A.; Kast, A. K.; Schröder, R. R.; Mankel, E.; Pingel, P.; Neher, D.; et al. Charge-Transfer-Solvent Interaction Predefines Doping Efficiency in p-Doped P3HT Films. *Chem. Mater.* **2016**, *28*, 4432-4439.

(8) Jacobs, I. E.; Aasen, E. W.; Oliveira, J. L.; Fonseca, T. N.; Roehling, J. D.; Li, J.; Zhang, G.; Augustine, M. P.; Mascal, M.; Moule, A. Comparison of Solution-Mixed and Sequentially Processed P3HT:F4TCNQ Films: Effect of Doping-Induced Aggregation on Film Morphology. *J. Mater. Chem. C* **2016**, *4*, 3454-3466.

(9) Shen, X.; Hu, W.; Russell, T. P. Measuring the Degree of Crystallinity in Semicrystalline Regioregular Poly(3-Hexylthiophene). *Macromolecules* **2016**, *49*, 4501-4509.

(10) Wojdyr, M. Fityk : A General-Purpose Peak Fitting Program. *J. Appl. Crystallogr.* **2010**, *43*, 1126-1228.

(11) Kresse, G.; Furthmüller, J. Efficiency of Ab-Initio Total Energy Calculations for Metals and Semiconductors Using a Plane-Wave Basis Set. *Comput. Mater. Sci.* **1996**, *6*, 15-50.

(12) Kresse, G.; Furthmüller, J. Efficient Iterative Schemes for Ab Initio Total-Energy Calculations Using a Plane-Wave Basis Set. *Phys. Rev. B - Condens. Matter Mater. Phys.* **1996**, *54*, 11169-11186.

(13) Perdew, J. P.; Burke, K.; Ernzerhof, M. Generalized Gradient Approximation Made Simple. *Phys. Rev. Lett.* **1996**, *77*, 3865-3868.

(14) Grimme, S.; Antony, J.; Ehrlich, S.; Krieg, H. A Consistent and Accurate Ab Initio Parametrization of Density Functional Dispersion Correction (DFT-D) for the 94 Elements

H-Pu. *J. Chem. Phys.* **2010**, *132*, 154104.

(15) Grimme, S.; Ehrlich, S.; Goerigk, L. Effect of the Damping Function in Dispersion Corrected Density Functional Theory. *J. Comput. Chem.* **2011**, *32*, 1456-1465.

(16) Dag, S.; Wang, L. W. Packing Structure of Poly(3-Hexylthiophene) Crystal: Ab Initio and Molecular Dynamics Studies. *J. Phys. Chem. B* **2010**, *114*, 5997-6000.

(17) Hopffgarten, M. von; Frenking, G. Energy Decomposition Analysis. *Wiley Interdiscip. Rev. Comput. Mol. Sci.* **2012**, *2*, 43-62.

(18) Su, P.; Li, H. Energy Decomposition Analysis of Covalent Bonds and Intermolecular Interactions. *J. Chem. Phys.* **2009**, *131*, 014102.

(19) Becke, A. D. Density-Functional Thermochemistry. III. The Role of Exact Exchange. *J. Chem. Phys.* **1993**, *98*, 5648-5652.

(20) Lee, C.; Yang, W.; Parr, R. G. Development of the Colle-Salvetti Correlation-Energy Formula into a Functional of the Electron Density. *Phys. Rev. B* **1988**, *37*, 785-789.

(21) Vosko, S. H.; Wilk, L.; Nusair, M. Accurate Spin-Dependent Electron Liquid Correlation Energies for Local Spin Density Calculations: A Critical Analysis. *Can. J. Phys.* **1980**, *58*, 1200-1211.

(22) Stephens, P. J.; Devlin, F. J.; Chabalowski, C. F.; Frisch, M. J. Ab Initio Calculation of Vibrational Absorption and Circular Dichroism Spectra Using Density Functional Force Fields. *J. Phys. Chem.* **1994**, *98*, 11623-11627.

(23) Schäfer, A.; Huber, C.; Ahlrichs, R. Fully Optimized Contracted Gaussian Basis Sets of Triple Zeta Valence Quality for Atoms Li to Kr. *J. Chem. Phys.* **1994**, *100*, 5829-5835.